ACS ES&T Engineering

pubs.acs.org/estengg

Article

Polyamide Nanofiltration Membranes from Emulsion-Mediated Interfacial Polymerization

Yuanzhe Liang, Xiangxiu Teng, Rui Chen, Yuzhang Zhu,* Jian Jin,* and Shihong Lin*

Cite This: *ACS EST Engg.* 2021, 1, 533−542

Read Online

ACCESS | Metrics & More | Article Recommendations | Supporting Information

ABSTRACT: Fabrication of nanofiltration (NF) membranes using interfacial polymerization (IP) continues to receive tremendous interest in research and development due to the broad applications of NF in water treatment, wastewater reuse, and industrial separations. Many approaches have been explored to enhance the performance of NF membranes by regulating the IP process. Among these approaches, the use of surfactants has shown strong potential due to its low cost and compatibility with existing infrastructure for membrane fabrication. While the different roles of the surfactants have been increasingly elucidated in recent years, little is known for the role of emulsion formation in the IP process. In this study, we investigate the impacts of nonionic, emulsifying surfactants on the formation, properties, and performance of the polyamide NF membranes. Two surfactants were compared, including the hydrophilic Tween 80, which is an oil-in-water (o/w) emulsifier added in the aqueous solution of piperazine, and the lipophilic Span 80, which is a water-in-oil (w/o) emulsifier added in the hexane solution of trimesoyl chloride. Our results illustrate the effects of emulsions as "vehicles" to facilitate monomer transfer and as "microreactors" for providing additional and distributed interfaces for IP. Depending on whether the surfactants are o/w or w/o emulsifiers, the resulting membranes have unique physicochemical properties and NF performance. In both cases, the addition of nonionic surfactants at low-to-moderate concentrations results in smaller pore sizes and a narrower pore size distribution. Overall, this study provides important insights into how the IP process and the resulting NF membranes are influenced by the formation of emulsions.

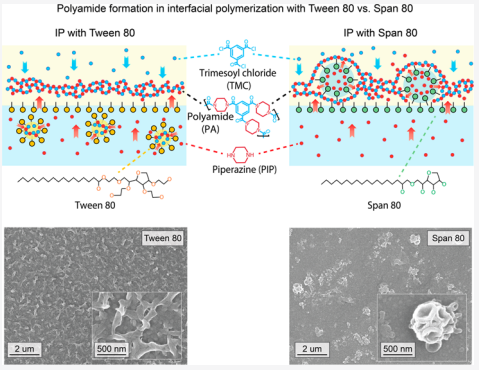

KEYWORDS: *Interfacial polymerization, Emulsion, Nonionic surfactant, Thin-film-composite polyamide membrane, Nanofiltration*

INTRODUCTION

Growing water scarcity is one of the leading challenges of our time, impacting over one-third of the world's population.[1,2] To address this challenge, research has been actively performed to explore more effective ways of tapping into unconventional sources to augment drinking water supply and/or reusing wastewater to reduce water demand.[2−5] Among the various technical approaches, membrane-based water and wastewater treatment technologies have received tremendous interest due to their small footprint, high energy efficiency, modularity, and capability of achieving molecular separation.[2,6−8] Specifically, nanofiltration (NF) is a low-pressure membrane-based process that is widely used in brackish water desalination and wastewater reclamation.[9,10] Compared to reverse osmosis (RO) membranes used widely for seawater desalination, the NF membrane typically has a relatively "loose" active layer that enables operation at a lower pressure and/or a higher flux.[11] More importantly, NF can also be employed for selective separation of solutes from a mixed solution based on the various solute exclusion mechanisms.[12,13]

Most commercial NF (and RO) membranes are thin-film-composite (TFC) polyamide membranes formed via a process called interfacial polymerization (IP).[14,15] In an IP process for making NF membranes, a hexane solution of trimesoyl chloride (TMC) is brought into contact with a porous support (typically an ultrafiltration membrane) prewetted with an aqueous solution of piperazine (PIP). The PIP molecules diffuse across the water−hexane interface and react with the TMC in the hexane phase to form a thin polyamide (PA) layer that serves as the active separation layer.[16] While there exist other methods for fabricating NF/RO membranes, the IP process is the most widely used in the industry because of its high manufacturing efficiency and the robust separation performance of the resulting TFC-PA membrane.[9,17−19]

Conventional IP fails to provide effective control of the membrane pore structure (e.g., pore size and thickness) due to uncontrolled trans-interface diffusion of PIP monomers and the fast polymerization between PIP and TMC, which lead to the formation of a polyamide active layer with multiscale

Received: November 9, 2020
Revised: December 28, 2020
Accepted: December 29, 2020
Published: January 8, 2021

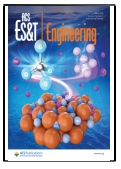

https://dx.doi.org/10.1021/acsestengg.0c00213
ACS EST Engg. 2021, 1, 533−542

heterogeneity and a large distribution of pore size.[20−24] Fundamental understanding of the IP process continues to attract research interests due to the wide industrial application of TFC-PA NF membranes.[10,25] Extensive research efforts have been devoted to modulate the IP process to achieve TFC-PA membranes with improved performance and desired properties.[18] For example, the properties and performance of TFC-PA membranes can be controlled by using different monomers and additives (including nanomaterials) and adjusting their concentrations.[26−29] Moreover, the environmental conditions for the fabrication also play an important role in controlling the properties and performance of the resulting membranes.[11,30]

One effective approach for modulating the IP process and the properties of the resulting TFC-PA membranes is by adding surfactants.[31−33] The roles of surfactants are multifaceted and dependent on the specific system. The most apparent role is to reduce the surface tension and thereby promote the wetting of the support layer and stabilize the water/oil interface.[33−37] It was found in previous studies that the presence of surfactants has a substantial impact on the morphology of the resulting PA layer formed from the polymerization between PIP and TMC, which alters the membrane permeability.[38] More recently, an additional role of surfactants in regulating the cross-interface transport of PIP has been recently proposed.[31] Specifically, it has been suggested that anionic surfactants, such as sodium dodecyl sulfate (SDS), which form a self-assembled dynamic 2D network at the water−hexane interface, can promote the kinetics and homogeneity of the PIP transport across the interface and result in a PA membrane with more uniform pore sizes for precise molecular separation.[31]

In addition to these effects, some surfactants are also known to be good emulsifiers.[39−41] The effects of emulsifying surfactants on the IP process, and the properties and performance of the resulting TFC-PA membrane have not been systematically investigated. The theory on how the chemical structure of surfactants affects their emulsifying behavior has been introduced by Griffin who proposed to use a parameter called the hydrophile−lipophile balance (HLB) to estimate the emulsification behavior of surfacants.[41] Surfactants with different HLB values have a different affinity (or solubility) toward either the water or the oil phase, which results in different emulsification behaviors. Specifically, surfactants with an HLB value from 8 to 16 (an approximate range) are effective oil in water (o/w) emulsifiers, whereas surfactants with an HLB value of 3−6 are effective water in oil (w/o) emulsifiers.[40,41] Effective emulsifiers of either kind (o/w or w/o) will likely promote the formation of emulsions near the water/hexane interface and thus affect the IP process, which in turn affects the properties and performance of the TFC-PA membranes.

In this study, we investigate the impacts of nonionic surfactants on the formation and properties of the TFC-PA NF membranes. The nonionic surfactants investigated include Tween 80 (HLB = 15) and Span 80 (HLB = 4.3). These two nonionic surfactants were chosen because (1) they have the proper HLBs as o/w and w/o emulsifiers, respectively, and (2) the absence of charge in these surfactants minimizes the complication of the surfactant charge effect in the IP and allows us to focus the analysis on the emulsification effect. We first fabricate the TFC-PA NF membranes with PIP and TMC using interfacial polymerization in the presence of either of the two surfactants and compare the resulting membranes to a reference TFC-PA NF membrane prepared without any surfactant. We then characterize the surface properties of these membranes and evaluate their NF performance in terms of water permeance and salt rejection. By comparing TFC-PA membranes fabricated with and without emulsifying agents, we aim to elucidate the impacts of emulsion formation on interfacial polymerization and the properties and NF performance of the resulting PA membranes.

MATERIAL AND METHODS

Materials and Chemicals. Piperazine (PIP, 99%), trimesoyl chloride (TMC, >98%), polysorbate 80 (Tween 80, BioXtra, Mw ∼ 1310), sorbitan oleate (Span 80, Mw ∼ 428), beta-carotene (≥93%, oil soluble-dye), basic dye (meta phenylene blue bb c.i. 50255, water-soluble dye), glycerol (≥99%), anhydrous D-(+)-glucose, sucrose (≥99.5%), D-(+)-Raffinose pentahydrate (≥98%), Na_2SO_4 (≥99%), $MgSO_4$ (≥99.5%), $MgCl_2$ (≥99.99%), $CaCl_2$ (≥97%), and NaCl (≥99%) were purchased from Sigma-Aldrich (St. Louis, MO) and were all used as received. Anhydrous *N*-hexane and ethanol (HPLC) were purchased from Fisher Scientific. The polyester sulfone ultrafiltration (NADIR UH050, MWCO 50000 Da) membrane was purchased from Microdyn-Nadir (Germany).

Preparation of the Polyamide Nanofiltration Membrane via Interfacial Polymerization. The reference TFC-PA NF membrane was prepared using piperazine (PIP, 0.25% (w/v) aqueous solution) and trimesoyl chloride (TMC, 0.2% (w/v) in *n*-hexane) on a commercial poly(ether sulfone) (PES) ultrafiltration (UF) membrane as the support layer via conventional interfacial polymerization (IP). The concentrations of PIP and TMC remained the same in the following discussion. In a standard IP process, the PES UF support membrane was first placed on a glass plate, and the surface of the UF membrane was impregnated with the aqueous PIP solution for 30 s. The excess PIP solution was then gently removed from the UF support membrane surface using a rubber roller. Next, a hexane solution of TMC was poured onto the UF membrane surface and kept still for another 30 s, which resulted in the formation of a thin PA active layer over the PES support membrane surface. The resulting TFC-PA membrane was rinsed with excessive *n*-hexane to remove unreacted TMC from the surface and then cured in an oven at 60 °C for 30 min to increase the degree of cross-linking. After curing, the TFC-PA membrane was stored in DI water at 4 °C to facilitate the hydrolysis of unreacted chloride groups in the polyamide network.

To investigate the effect of nonionic surfactants on interfacial polymerization and the resulting TFC-PA membranes, the hydrophilic nonionic surfactant was added into the PIP solution for impregnating the PES support layer, whereas the lipophilic nonionic surfactant was added in the TMC hexane solution. The first nonionic surfactant, Tween 80, has a hydrophilic−lipophilic balance (HLB) value of 15 and is thus considered a good oil-in-water emulsifier.[40] The second nonionic surfactant, Span 80, has an HLB value of 4.3 and is thus considered a good water-in-oil emulsifier.[41] The concentrations of Tween 80 (in water) and Span 80 (in hexane) vary from 0% (w/v) to 0.5% (w/v) to evaluate the effect of surfactant concentration on the resulting polyamide nanofiltration membrane.

Membrane Characterization. We characterized the surface potentials of the TFC-PA NF membranes using a

https://dx.doi.org/10.1021/acsestengg.0c00213
ACS EST Engg. 2021, 1, 533−542

streaming potential analyzer (SurPASS electrokinetic analyzer, Anton Paar, Ashland, VA) with a background polyelectrolyte of 1 mM KCl solution. We also measured the water contact angle (WCA) of the TFC-PA membranes using an optical tensiometer (Theta Lite, Biolin Scientific). Scanning electron microscope (SEM) imaging was performed to characterize the surface morphology of the TFC-PA NF membranes using a high-resolution Zeiss Merlin SEM equipped with a GEMINI II column with an accelerating voltage of 3 kV. All SEM membrane samples were sputter-coated with a 5 nm gold coating to avoid the charging effect. X-ray photoelectron spectrometry (XPS) was performed using an X-ray photoelectron spectrometer (ESCALAB 250 Xi, Thermal Fisher Scientific) to obtain the surface elemental compositions of polyamide active layers prepared from conventional IP and IP with nonionic surfactants. The chemical structure of the TFC-PA NF membranes was also investigated using Fourier transform infrared spectrometer (Bruker Tensor 27). Transmittance spectra were collected ranging from 800 to 4000 cm^{-1} at a resolution of 2 cm^{-1} for 256 scans.

To evaluate the pore size distribution of the TFC-PA NF membranes, we performed filtration experiments with a series of neutral organic molecules (e.g., glycerol (92 Da), glucose (180 Da), sucrose (342 Da), raffinose (504 Da)) using a custom cross-flow NF system. The feed concentration was 200 ppm for all species, and the applied pressure was 4 bar. We collected feed and permeate samples and measured the total organic carbon (TOC) using a TOC analyzer (Aurora Model 1030, OI Analytical, Inc.) to determine the organic concentrations of the feed and permeate samples. The MWCO and pore size information on the TFC-PA NF membranes were calculated using the rejection of the organic solutes. Specifically, the MWCO of the membrane is defined as the molecular weight of solute with a rejection of 90%, whereas the mean pore size corresponds to the Stokes radius of the neutral solute with a measured rejection rate of 50%. The pore size distribution of the TFC-PA NF membrane is expressed as the geometric standard deviation of the probability density function (PDF) curve (eq 1), which is the ratio of the stokes radius with a rejection of 84.13% to that with a rejection of 50%.[42]

$$\frac{dR(r_p)}{dr_p} = \frac{1}{r_p \ln \sigma_p \sqrt{2\pi}} \exp\left[-\frac{(\ln r_p - \ln \mu_p)^2}{2(\ln \sigma_p)^2}\right] \quad (1)$$

where μ_p is the mean pore size, σ_p is the geometric standard deviation of the PDF curve, and r_p is the Stokes radius of the organic solute. The Stokes radii of these molecules correlate with their molecular weight[42] (eq 2):

$$\ln(r_p) = -1.496 + 0.465 \ln(MW) \quad (2)$$

where MW is the molecular weight of each organic solute. Based on this correlation, the Stokes radii for glycerol, glucose, sucrose, and raffinose are 0.261, 0.359, 0.462, and 0.538 nm, respectively.

Dye-Partitioning at the Water/Hexane Interface. We performed dye partitioning experiments to investigate how solutes in one phase partition to another phase in the presence of surfactants. Specifically, we used a water-soluble dye (blue) in the aqueous solution to mimic the partitioning of PIP from water into hexane during the IP process. We also used a lipid-soluble dye (yellow) in the hexane to mimic the partitioning of TMC from hexane into the water during the IP. In all cases, water was first placed in a beaker, and then hexane was added on top of the water using a transfer pipet. Each of the two phases (water or hexane) may or may not contain dyes or surfactants, with all the experimental scenarios summarized in Table 1. The mixing behavior upon adding hexane to water was recorded with both photos and videos.

Table 1. Summary of Dye-Partitioning Experiments

type of surfactant	experiment no.	components in each phase: water phase	components in each phase: hexane phase
Tween 80	1-1	none	dye (yellow)
	1-2	Tween 80	dye (yellow)
	1-3	Tween 80, dye (blue)	none
Span 80	2-1	dye (blue)	none
	2-2	dye (blue)	Span 80
	2-3	none	Span 80, dye (yellow)

Nanofiltration Performance Evaluation. The performance matrix including permeance and salt rejection of the TFC-PA NF membranes was evaluated using a custom-made crossflow filtration system (Figure S1). The crossflow system contains three stainless steel membrane testing cells connected in parallel. Three membranes were mounted into each of the three cells and tested simultaneously. Each cell has an active membrane area of 7.1 cm^2. The feed solution encounters a 90° degree bend when it enters the cell inlet. The crossflow velocity was 2.5 cm s^{-1}, and the applied pressure was 4 bar. All membranes were compacted with deionized water overnight prior to any test with a salt solution. Membrane permeance and salt selectivity were evaluated with five types of common salt solutions (1000 ppm), including Na_2SO_4, $MgSO_4$, $MgCl_2$, $CaCl_2$, and NaCl. The solution temperature was maintained at 25 °C during the test. All measurements were carried out when the filtration process becomes stable. The permeance of the TFC-PA NF membrane, P (L m^{-2} h^{-1} bar^{-1}), was determined using the following equation:

$$P = \frac{J}{\Delta P} \quad (3)$$

where J is the volumetric flux of water (L m^{-2} h^{-1}) and ΔP is the applied pressure (bar), respectively. The rejection of solute by the TFC-PA NF membrane was determined by measuring the steady-state electrical conductivity of the feed and permeate solution using the following equation.

$$R = \left(1 - \frac{c_p}{c_f}\right) \times 100\% \quad (4)$$

where c_p and c_f are the solute concentrations of the permeate and feed solutions, respectively,

RESULTS AND DISCUSSION

Membrane Surface Morphology Depends on Surfactant Type. The addition of hydrophilic and lipophilic surfactants in IP has a substantial impact on the surface morphology of the resulting TFC-PA NF membranes (Figure 1). As a baseline, the reference TFC-PA NF membrane prepared from conventional IP (without any surfactant) has a

https://dx.doi.org/10.1021/acsestengg.0c00213
ACS EST Engg. 2021, 1, 533−542

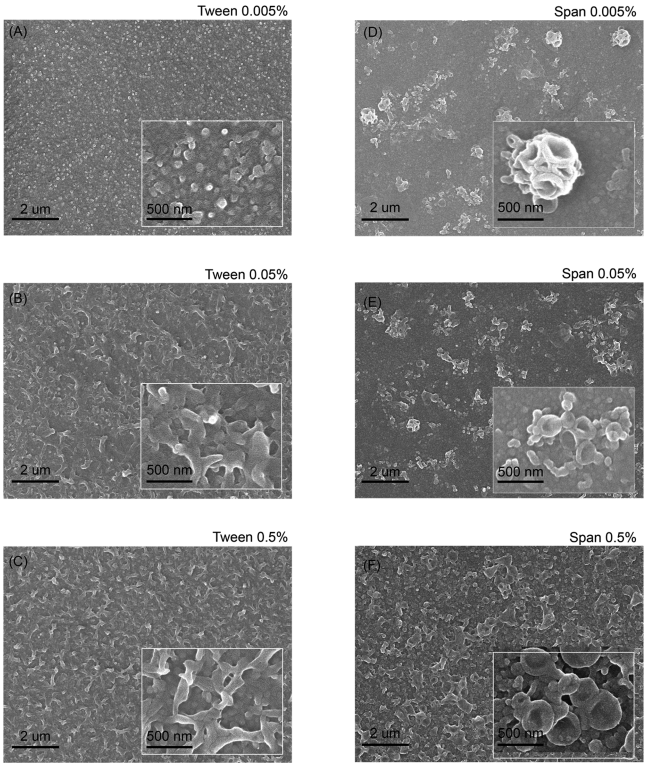

Figure 1. SEM images of the surface morphology of TFC-PA NF membranes formed via IP with the addition of (A, B, C) the hydrophilic nonionic surfactant (Tween 80) and (D, E, F) the lipophilic nonionic surfactant (Span 80) as a function of surfactant concentrations.

relatively smooth surface (Figure S2). The addition of hydrophilic nonionic surfactants (Tween 80) in the PIP solution leads to the formation of nodular structures on the PA surface (Figure 1A). As the Tween 80 concentration increases from 0.005% (w/v) to 0.05% (w/v) in the PIP solution, the nodular structure transforms into a crumpled structure (Figure 1B) and the density of the crumpled structure increases with increasing the Tween 80 concentration (Figure 1C). The formation of nodular and crumpled structures is attributed to the enhanced wetting of the PIP solution on the PES UF substrate in the presence of Tween 80 (Figure S3).[38] In comparison, the addition of lipophilic nonionic surfactants (Span 80) in the *n*-hexane solution of TMC yields structures of deflated spheres on the PA surface (Figure 1D). The areal number density of the deflated structures increases with increasing Span 80 concentration (Figure 1E). At sufficiently high Span 80 concentration, these deflated spherical structures become interconnected (Figure 1F).

Membrane Surface Properties Depend on Surfactant Type. The streaming potential measurements reveal no discernible difference between the zeta potentials of the reference TFC-PA NF membrane prepared via conventional IP and the TFC-PA NF membrane prepared via IP with Tween 80 added in the PIP solution (Figure 2A), suggesting that the addition of Tween 80 in the IP reaction did not alter the surface functional groups of the polyamide active layer. However, the addition of Span 80 in the TMC solution results in a noticeable reduction of the absolute values of the surface potential (i.e., the addition of Span 80 in IP reaction makes the TFC-PA membrane less charged) but without shifting the isoelectric point (IPE), which is likely caused by the reduction of the areal density of the surface carboxylic groups due to the integration of the uncharged Span 80 in the PA structure (including the surface). The addition of nonionic surfactants in the IP process also has a substantial impact on the wetting property of the resulting TFC-PA membrane (Figure 2B). Specifically, the presence of Span 80 increased the water contact angle (WCA) systematically with a higher Span 80 concentration (in hexane) leading to a higher WCA. In comparison, the addition of Tween 80 has a less significant effect on the surface wetting property. Specifically, increasing the dosing concentration of Tween 80 (in water) first slightly reduced the WCA but then increased the WCA when the Tween 80 concentration exceeded 0.125% (w/v).

The elemental composition of the TFC-PA surface is also dependent on both the type and concentration of the dosing surfactants. Analyzing the XPS spectra of the surface of the TFC-PA membranes fabricated using different conditions (Figure 2C,D) suggests the possible integration of surfactants into the PA matrix. Specifically, the N/O ratio decreased systematically with an increasing Span 80 concentration (Table 2). When Tween 80 was the dosing agent, the N/O ratio first increased and then decreased when the concentration exceeded 0.125% (w/v) (Table 2). The integration of Tween 80 in the PA layer is further confirmed by the FT-IR analysis of the reference TFC-PA membrane and the TFC-PA membrane prepared from IP with Tween 80 (Figure S4). Specifically, the appearance of additional characteristic peaks at 1735 and 1098 cm^{-1} is associated with the C═O stretching and the C−O−C stretching of the ester group.[43,44]

Interestingly, the WCA (Figure 2B) negatively correlates with the N/O ratio (Table 1) in a semiquantitative way for both Tween 80 and Span 80 (Figure S5). We note that while the N/O ratio is often used in characterizing the degree of cross-linking in PA, it cannot be used for this purpose here due to the potential integration of nonionic surfactants that may contribute substantially to the N/O ratio. The TFC-PA membranes prepared from IP with Span 80 exhibited an increase in the surface hydrophobicity (WCA) and a decrease in the N/O ratio even at an extremely low Span 80 concentration (0.005% (w/v)). Increasing Span 80 concentration made the membrane more hydrophobic and reduced the N/O ratio because of the more Span 80 integrated into the PA matrix, which is also consistent with the observation of reduced absolute values of the surface potential for the TFC-PA membrane prepared using Span. In comparison, very little Tween 80 integration in the polyamide matrix was observed at low Tween 80 concentrations (below 0.25% (w/v)), as the N/O ratio remains nearly constant. The slight decrease in WCA may come from the increase in surface roughness (Figure 1A–C, Figure S2), as consistent with Wenzel's theory.[45]

The primary difference between Span 80 and Tween 80 in their effectiveness in altering the PA composition and properties can be explained by the fact that Span 80 was present in the hexane phase where PA forms. While the formation of PA is referred to as "interfacial polymerization", multiple previous studies have suggested that the polymerization occurs in the "hexane side" of the interface.[20,21,23] Because Span 80 is soluble in hexane and was dosed in hexane, it is likely integrated into the PA layer formed in the hexane phase. In comparison, Tween 80 is barely soluble in hexane and was added to the aqueous solution. For this reason, it is substantially less likely that Tween 80 molecules could be integrated into the PA layer, especially considering that IP is a

https://dx.doi.org/10.1021/acsestengg.0c00213
ACS EST Engg. 2021, 1, 533−542

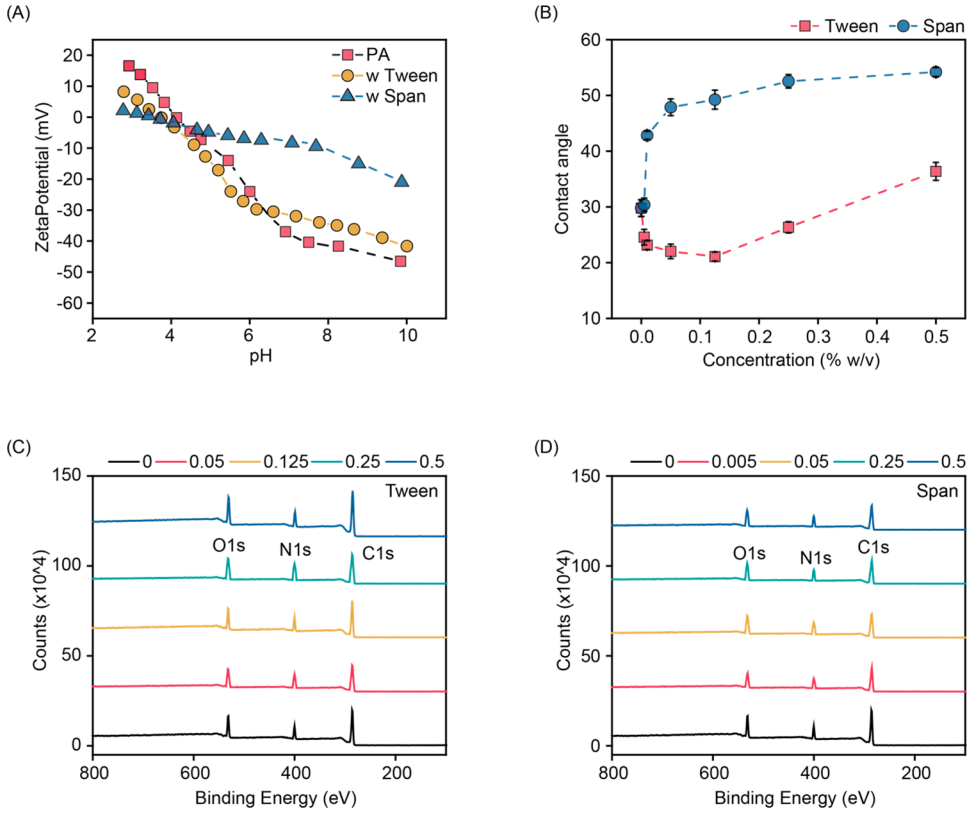

Figure 2. (A) Surface streaming potential of TFC-PA membranes prepared from IP and IP with the addition of the hydrophilic nonionic surfactant (Tween 80) and the lipophilic nonionic surfactant (Span 80). (B) Water contact angle of TFC-PA NF membrane formed via IP with the addition of the hydrophilic nonionic surfactant (Tween 80) and the lipophilic nonionic surfactant (Span 80) as a function of surfactant concentrations. XPS survey of polyamide active layer formed via IP with the addition of (C) the hydrophilic nonionic surfactant (Tween 80) and (D) the lipophilic nonionic surfactant (Span 80) as a function of surfactant concentrations.

Table 2. Elemental Composition of the PA Layer Formed from IP with Tween 80 and Span 80

membrane type		C (%)	N (%)	O (%)	N/O (%)
reference (no surfactant added)		70.24	13.63	15.96	85.4
Tween 80	0.05% (w/v)	70.37	13.71	15.87	86.4
	0.125% (w/v)	71.04	13.37	15.24	87.7
	0.25% (w/v)	70.90	13.36	15.55	85.9
	0.5% (w/v)	71.38	12.68	15.81	80.2
Span 80	0.005% (w/v)	73.40	11.32	15.08	75.1
	0.05% (w/v)	69.52	12.40	18.08	68.6
	0.25% (w/v)	71.41	11.03	17.55	62.8
	0.5% (w/v)	73.62	10.00	16.38	61.0

rather rapid and self-terminating process. Based on the results of both the WCA and N/O values, a small degree of Tween 80 integration was observed only when the Tween 80 concentration exceeded 0.25% (w/v). The above explanation on the effect of the surfactants in PA membrane properties focuses primarily on whether the surfactant molecules exist in the hexane phase where PA is formed. However, surfactants may have an additional effect via the formation of emulsions, which will be discussed in the following section.

Emulsions as Vehicles and Microreactors. Like all other surfactants, Tween 80 also promotes better wetting of the support layer (Supporting Information Figure S3), and both Tween 80 and Span 80 reduce the interfacial tension between water and hexane (Figure 3A). However, Tween 80 and Span 80 differ from some common surfactants in that their HLB values fall into the ranges of effective emulsifiers.[39] For example, Tween 80 (HLB ~ 15) is a good oil-in-water (o/w) emulsifier (HLB range: 8−18), whereas Span 80 (HLB ~ 4.3) is a good water-in-oil (w/o) emulsifier (HLB range: 4−6). To illustrate the effectiveness of these surfactants in emulsification, we performed experiments to show the stability of the oil/water interface when the surfactants are added into one of the two phases. Specifically, the oil phase was dosed with an orange, water-insoluble dye (beta carotene), and the water phase was dosed with a blue, oil-insoluble dye (meta phenylene blue) to clearly show the oil/water interface.

With no surfactants added, the water/hexane interface was relatively clear and stable (Figure 3B,E). No oil dye partitions into the clear water phase (Figure 3B), and no water dye partitions into the clear oil phase (Figure 3E). When Tween 80 was added into the clear (undyed) water phase which was put into contact with the hexane phase containing orange dye, the water phase became muddy and orange, which indicates the formation of the o/w emulsion containing the orange dye (Figure 3C). Similarly, when Span 80 was added into the transparent hexane phase which was put into contact with the blue-dyed water phase, the hexane phase also showed clear evidence of the formation of w/o emulsions containing the blue dye (Figure 3F).

In the experiments shown in Figure 3C,F, the dyes and the surfactants were added into different phases, which does not clearly show if emulsions also formed in the dyed phase. Therefore, we performed additional experiments where dyes and surfactants were added in the same phase. Specifically,

https://dx.doi.org/10.1021/acsestengg.0c00213
ACS EST Engg. 2021, 1, 533−542

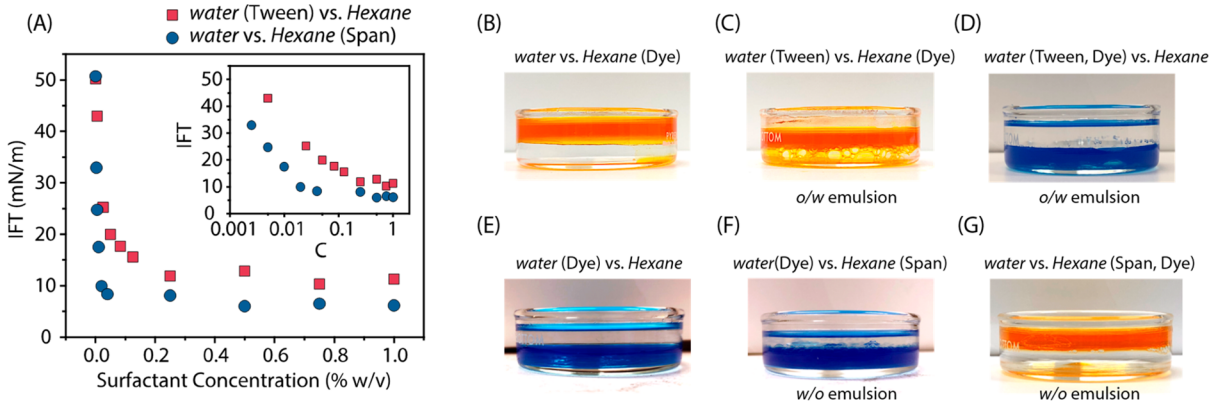

Figure 3. (A) Interfacial surface tension of water and hexane as a function of Tween 80 concentration in water (red square) or Span 80 concentration in hexane (blue circle). Demonstration of the presence of Tween 80 in water leading to the formation of an oil-in-water emulsion upon mixing of water and hexane. (B) Control experiment: when Tween 80 is absent, no emulsion (yellow color) is observed in water. (C) The presence of Tween 80 results in the formation of an oil-in-water emulsion (yellow bubbles) in water. (D) Control experiment: Tween 80 does not lead to the formation of a water-in-oil emulsion (no blue color) in hexane. Demonstration of the presence of Span 80 in hexane leading to the formation of a water-in-oil emulsion upon mixing of water and hexane. (E) Control experiment: when Span 80 is absent, no color (emulsion) is observed in hexane. (F) The presence of Span 80 results in the formation of a water-in-oil emulsion (blue bubbles) in hexane. (G) Control experiment: Span 80 does not lead to the formation of an oil-in-water emulsion (no yellow color) in water.

when both Tween 80 and water-soluble dye were added into water, no formation of the blue emulsion was observed in the clear oil phase (Figure 3D). The absence of emulsification in the oil phase is attributable to the fact that Tween 80, being a good o/w emulsifier, is a poor w/o emulsifier. Similarly, when both Span 80 and the oil-soluble dye were added into the oil phase, no o/w emulsion was observed in the water phase (Figure 3G), because Span 80, though being an effective w/o emulsifier, is a poor o/w emulsifier.

The emulsification behaviors in the presence of nonionic surfactants as illustrated using dyed solutions provide important insights into how interfacial polymerization (IP) can be affected by these surfactants. Specifically, we consider the effect of monomer transporting via emulsions containing those monomers, i.e., the emulsions serve as "vehicles" to bring the monomers into another phase (Figure 4). For example, when Tween 80 was added into the PIP solution, o/w emulsions formed in the aqueous solution brought the emulsified oil droplets containing TMC into the water phase

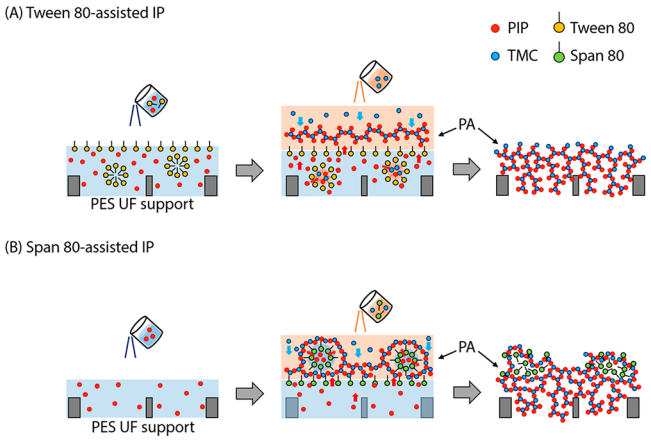

Figure 4. Schematic illustration of the polyamide active layer formation via IP with the addition of (A) the hydrophilic nonionic surfactant (Tween 80) and (B) the lipophilic nonionic surfactant (Span 80).

(Figure 4A). These emulsified oil droplets served as microreactors for local interfacial polymerization that led to the formation of short PA fragments. These disconnected segments forming in the water phase were unlikely to be integrated into the continuous PA layer formed on the hexane side of the water/hexane interface. Instead, these segments were likely subject to fast hydrolysis, became embedded underneath the PA active layer, and had limited impact on the properties of the PA layer.

In fact, the streaming potential measurements reveal almost no difference in surface potential between the PA layers formed with and without Tween 80 (Figure 2A). The presence of Tween 80 has a relatively small impact (as compared to Span 80 to be discussed) on the WCA and elemental composition of the PA layer (Figure 2B,C and Table 2), which is likely attributable to the integration of Tween 80 in the PA layer. We note that the integration of a small amount of Tween 80 does not affect the surface potential of the PA layer because Tween 80 does not partition into the hexane phase and is thus not present on and near the surface of the resulting PA layer. Similarly, the changes in WCA and elemental composition were hardly observed if oil-insoluble and nonemulsifying surfactants (e.g., SDS or SDBS) were used.[31] These observations are all consistent with the above hypothesis regarding how Tween 80 may affect the PA formation. Lastly, the emergence of the nodular and crumpled structures (Figure 1A–C) results from the improved wetting of the PES substrate by the surfactant-dosed PIP solution, which has been well elaborated in the work by Niu et al.[38]

In comparison, adding Span 80 into the hexane TMC solution has a very different impact on interfacial polymerization. As Span 80 is a highly effective w/o emulsifier, PIP encapsulated in water-in-hexane (w/o) emulsions is transported to the hexane phase via the "vehicle effect" (Figure 4B). The emulsion-facilitated transport of PIP adds to the trans-interface diffusion of PIP from water to hexane. These w/o emulsions also serve as microreactors for interfacial polymerization. In this case, however, the PA formed around the emulsified water droplets because PA tends to form in the hexane side of the water/hexane interface. These PA fragments

https://dx.doi.org/10.1021/acsestengg.0c00213
ACS EST Engg. 2021, 1, 533–542

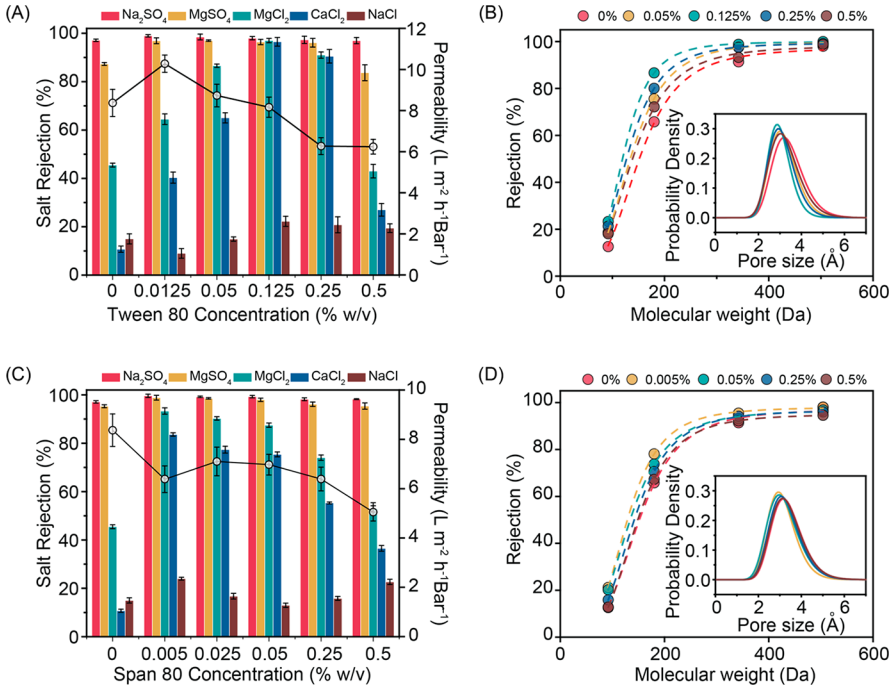

Figure 5. (A) Pure water permeability (line) and rejection of different salts (columns) by the TFC-PA membranes (prepared by adding Tween 80 in the PIP solution) as a function of the Tween 80 concentration. (B) Rejection of uncharged organic molecules including glycerol, glucose, sucrose, and raffinose by TFC-PA membranes prepared using different Tween 80 concentrations. Inset: pore size distribution of the PA-TFC NF membranes as derived from the rejection curves of uncharged organic molecules. (C) Pure water permeability (line) and rejection of different salts (columns) by the TFC-PA membranes (prepared by adding Span 80 in the PIP solution) as a function of the Span 80 concentration. (D) Rejection of uncharged organic molecules including glycerol, glucose, sucrose, and raffinose by TFC-PA membranes prepared using different Span 80 concentrations. Inset: pore size distribution of the PA-TFC NF membranes as derived from the rejection curves of uncharged organic molecules. All measurements were carried out at an applied pressure of 4 bar. Rejection and flux data are reported as the average of three runs, and the error bars represent the standard deviation.

are less susceptible to hydrolysis as they are in the hexane phase and are thus given the opportunity to continue to react with other PA fragments forming from the reaction between TMC and the PIP diffusing across the interface between the bulk water and bulk hexane. Eventually, these "PA vesicles" forming at the w/o emulsion interface merged with the PA film forming at the interface between the bulk phases. When the PA membrane was dried, the evaporation of water inside these vesicles led to the formation of collapsed vesicles as observed in Figure 1D–F. In this case, the Span 80 surfactants were trapped in the collapsed PA layers and contributed substantially to the chemical composition of the PA layer (Table 1) and the physical properties of the PA layers such as surface potential (Figure 2A) and WCA (Figure 2B).

Membrane Performance and Pore Structure. The additions of Tween 80 in water and Span 80 in hexane resulted in distinct membrane performances. When Tween 80 was added into the aqueous phase, the membrane permeability slightly increased at low Tween 80 concentration due to the creation of the crumpled structure on the membrane surface which increased the specific surface area and then decreased as the pore size of the TFC-PA membranes decreased at high Tween 80 concentrations (Figure 5A). The measured salt rejection of the TFC-PA NF membranes increased when the Tween 80 concentration increased from 0% (w/v) to 0.125% (w/v) (Figure 5A). But when the Tween 80 concentration exceeded 0.5% (w/v), the salt rejections for several salts (except Na_2SO_4) declined. The initial increase of the salt rejection was attributable to a reduction of the molecular weight cutoff (MWCO) of the TFC-PA membranes prepared in the presence of Tween 80 (Figure 5B and inset). In particular, the TFC-PA membranes prepared with a Tween 80 concentration of 0.125% (w/v) exhibited a remarkable performance for separating divalent and multivalent ions (e.g., Zn^{2+}, Mg^{2+}, SO_4^{2-}, $Fe(CN)_6^{3-}$, etc.) from monovalent salts (K^+, Na^+, NO_3^-, etc.) (Figure S6).

This enhancement in the solute separation precision by Tween 80 is similar to what has been observed in surfactant assembly regulated interfacial polymerization (SARIP) using SDS.[31] Similar to the sulfate group in SDS, Tween 80 has abundant hydroxyl groups on its hydrophilic end, which can attract the positively charged PIP molecules. Also, the self-assembled Tween 80 network at the water–hexane interface regulates the trans-interface diffusion of PIP from the water phase to the hexane phase and thereby improves the homogeneity of the pore size distribution of the resulting PA membrane (Table 3). However, when the Tween 80 concentration reached 0.5% (w/v), the separation performance became compromised as the rejections of divalent cations became substantially lower (Figure 5A) and the MWCO of the membrane became larger (Figure 5B).

The deterioration in performance at a relatively high Tween 80 concentration is likely attributable to the integration of Tween 80 molecules in the PA active layer as indicated by both the measured WCA (Figure 5B) and the active layer composition (Table 2). While the exact mechanism of Tween 80 integration into the PA network is unclear, we speculate that such an integration is attributable to both (1) the van der Waals interaction between the hydrocarbon chain of Tween 80 and PA and (2) the hydrogen bond between the

https://dx.doi.org/10.1021/acsestengg.0c00213
ACS EST Engg. 2021, 1, 533–542

Table 3. Mean Pore Size and Pore Size Distribution of the PA Layers Formed from IP with Tween 80 (in Water) and Span 80 (in Hexane)

membrane type		mean pore size (Å)	pore size distribution
reference (no surfactant added)		3.312	1.238
Tween 80	0.05%	3.126	1.222
	0.125%	2.956	1.189
	0.25%	3.046	1.217
	0.5%	3.175	1.245
Span 80	0.005%	3.064	1.233
	0.05%	3.124	1.258
	0.25%	3.209	1.241
	0.5%	3.28	1.243

hydroxyl groups of Tween 80 and the amine groups of the PIP (that are diffusing across the interface) and of the formed PA segments.

Adding a small concentration of Span 80 resulted in a substantial improvement of divalent cation rejection (Figure 5C), which is again likely attributable to the mechanism of SARIP. It requires a lower concentration of Span 80 than Tween 80 to induce similar enhancement in divalent cation rejection, which is likely because Span 80 has a higher surface excess concentration than Tween 80 (Figure 3A) and can thus form a denser interfacial surfactant network than Tween 80 at the same bulk concentration.[46] However, as Span 80 molecules were integrated into the PA network by an increasing extent with heightened Span 80 concentration, the rejection of divalent cations systematically decreased. Because of the hydrophobic nature of Span 80, the implantation of Span 80 inside the polyamide network led to a reduction of the membrane permeability due to the reduced surface hydrophilicity (Figure 2B). The changes of the MWCO and pore size distribution as a function of the Span 80 concentration also follow the same trend as that for divalent cation rejection (Figure 5D) and are in general consistent with the dependence of the membrane properties (water contact angles and elemental composition) on the Span 80 concentration (Figure 2B, Table 2). In other words, the addition of Span 80 has competing effects of SARIP and surfactant integration (into the PA network), with the former having a positive impact and the latter having a negative impact on the membrane pore size (Table 3), on the rejection of divalent cations, and on achieving precise selective ion separation.

CONCLUSION

We show in this comparative study how the addition of emulsifying nonionic surfactants in the IP process can affect the properties and nanofiltration performance of the resulting TFC-PA membranes. Our experimental results suggest that, in addition to the known effects of surfactants such as SARIP and improved wetting of the supporting layer, the formation of emulsions also has interesting impacts on the IP process. In particular, the addition into the hexane phase Span 80, which is an effective w/o emulsifier, has a substantial impact on the various properties (morphology, surface potential, wetting properties, and composition) and the NF performance of the resulting TFC-PA membranes via both the "vehicle effect" and integration of surfactants into the PA layer. Whereas, the addition of a hydrophilic nonionic surfactant, Tween 80, as an effective o/w emulsifier, reveals a qualitatively similar effect on the structure–performance properties of the resulting TFC-PA membranes as an anionic surfactant, SDS. This finding not only demonstrates the mechanism of nonionic surfactant-mediated IP but also provides additional guidance for the surfactant selection to tailor the structure and performance of TFC-PA NF membranes.

ASSOCIATED CONTENT

Supporting Information

The Supporting Information is available free of charge at https://pubs.acs.org/doi/10.1021/acsestengg.0c00213.

Figure S1, Custom-made crossflow NF testing system; Figure S2, SEM image of the surface morphology of TFC-PA NF membranes formed via conventional IP; Figure S3, contact angle of the PIP–Tween 80 aqueous solution on the PES UF substrate as a function of the Tween 80 concentration; Figure S4, FT-IR spectrum of the reference TFC-PA membrane prepared from conventional IP and the TFC-PA membrane prepared from IP with Tween 80; Figure S5, water contact angle and the N/O ratio of the TFC-PA NF membrane formed via IP with the addition of the hydrophilic nonionic surfactant (Tween 80) and the lipophilic nonionic surfactant (Span 80) as a function of surfactant concentrations; Figure S6, selectivity of different solutes as a function of Stokes radii for the PA-TFC NF membrane prepared via IP with 0.125% (w/v) Tween 80 in PIP solution (PDF)

AUTHOR INFORMATION

Corresponding Authors

Yuzhang Zhu – *i-Lab and CAS Center for Excellence in Nanoscience, Suzhou Institute of Nano-Tech and Nano-Bionics, Chinese Academy of Sciences, Suzhou 215123, P.R. China;* orcid.org/0000-0002-7279-2903; Email: yzzhu2011@sinano.ac.cn

Jian Jin – *i-Lab and CAS Center for Excellence in Nanoscience, Suzhou Institute of Nano-Tech and Nano-Bionics, Chinese Academy of Sciences, Suzhou 215123, P.R. China; College of Chemistry, Chemical Engineering and Materials Science, Soochow University, Suzhou 215123, P. R. China;* orcid.org/0000-0003-0429-300X; Email: jjin2009@sinano.ac.cn

Shihong Lin – *Department of Civil and Environmental Engineering and Interdisciplinary Material Science Program, Vanderbilt University, Nashville, Tennessee 37235-1831, United States;* orcid.org/0000-0001-9832-9127; Email: shihong.lin@vanderbilt.edu

Authors

Yuanzhe Liang – *i-Lab and CAS Center for Excellence in Nanoscience, Suzhou Institute of Nano-Tech and Nano-Bionics, Chinese Academy of Sciences, Suzhou 215123, P.R. China; Department of Civil and Environmental Engineering and Interdisciplinary Material Science Program, Vanderbilt University, Nashville, Tennessee 37235-1831, United States;* orcid.org/0000-0001-6197-1933

Xiangxiu Teng – *i-Lab and CAS Center for Excellence in Nanoscience, Suzhou Institute of Nano-Tech and Nano-Bionics, Chinese Academy of Sciences, Suzhou 215123, P.R. China*

Rui Chen − *Department of Civil and Environmental Engineering, Vanderbilt University, Nashville, Tennessee 37235-1831, United States*

Complete contact information is available at: https://pubs.acs.org/10.1021/acsestengg.0c00213

Notes

The authors declare no competing financial interest.

■ ACKNOWLEDGMENTS

This work is supported by the National Natural Science Funds for Distinguished Young Scholar (51625306) and the National Natural Science Foundation of China (21988102). S. Lin also acknowledges the partial support from U.S. National Science Foundation (CBET-2017998).

■ REFERENCES

(1) Elimelech, M.; Phillip, W. A. The Future of Seawater Desalination: Energy, Technology, and the Environment. *Science* **2011**, *333* (6043), 712−717.
(2) Shannon, M. A.; Bohn, P. W.; Elimelech, M.; Georgiadis, J. G.; Mariñas, B. J.; Mayes, A. M.Science and Technology for Water Purification in the Coming Decadess. *Nature*; **2008**, *452* 301−310. .
(3) Li, R.; Shi, Y.; Shi, L.; Alsaedi, M.; Wang, P. Harvesting Water from Air: Using Anhydrous Salt with Sunlight. *Environ. Sci. Technol.* **2018**, *52* (9), 5398−5406.
(4) Wang, R.; Zimmerman, J. B. Economic and Environmental Assessment of Office Building Rainwater Harvesting Systems in Various U.S. Cities. *Environ. Sci. Technol.* **2015**, *49* (3), 1768−1778.
(5) Misra, A. K. Climate Change and Challenges of Water and Food Security. *Int. J. Sustainable Built Environ.* **2014**, *3* (1), 153−165.
(6) Tang, C. Y.; Yang, Z.; Guo, H.; Wen, J. J.; Nghiem, L. D.; Cornelissen, E. Potable Water Reuse through Advanced Membrane Technology. *Environ. Sci. Technol.* **2018**, *52* (18), 10215−10223.
(7) Fane, A. G.; Wang, R.; Hu, M. X. Synthetic Membranes for Water Purification: Status and Future. *Angew. Chem., Int. Ed.* **2015**, *54* (11), 3368−3386.
(8) Werber, J. R.; Osuji, C. O.; Elimelech, M. Materials for Next-Generation Desalination and Water Purification Membranes. *Nature Reviews Materials.* **2016**, *1*, 16018.
(9) Mohammad, A. W.; Teow, Y. H.; Ang, W. L.; Chung, Y. T.; Oatley-Radcliffe, D. L.; Hilal, N. Nanofiltration Membranes Review: Recent Advances and Future Prospects. *Desalination* **2015**, *356*, 226−254.
(10) Hilal, N.; Al-Zoubi, H.; Darwish, N. A.; Mohamma, A. W.; Abu Arabi, M. A Comprehensive Review of Nanofiltration Membranes: Treatment, Pretreatment, Modelling, and Atomic Force Microscopy. *Desalination* **2004**, *170* (3), 281−308.
(11) Petersen, R. J. Composite Reverse Osmosis and Nanofiltration Membranes. *J. Membr. Sci.* **1993**, *83*, 81−150.
(12) Van Der Bruggen, B.; Vandecasteele, C. Removal of Pollutants from Surface Water and Groundwater by Nanofiltration: Overview of Possible Applications in the Drinking Water Industry. *Environ. Pollut.* **2003**, *122* (3), 435−445.
(13) Fernandes, P. A.; Cordeiro, M. N. D. S.; Gomes, J. A. N. F. Influence of Ion Size and Charge in Ion Transfer Processes Across a LiquidlLiquid Interface. *J. Phys. Chem. B* **2000**, *104* (10), 2278−2286.
(14) Cadotte, J. E.; Petersen, R. J.; Larson, R. E.; Erickson, E. E. A New Thin-Film Composite Seawater Reverse Osmosis Membrane. *Desalination* **1980**, *32* (C), 25−31.
(15) Cadotte, J. E.; King, R. S.; Majerle, R. J.; Petersen, R. J. Interfacial Synthesis in the Preparation of Reverse Osmosis Membranes. *J. Macromol. Sci., Chem.* **1981**, *15* (5), 727−755.
(16) Wang, Z.; Wang, Z.; Lin, S.; Jin, H.; Gao, S.; Zhu, Y.; Jin, J. Nanoparticle-Templated Nanofiltration Membranes for Ultrahigh Performance Desalination. *Nat. Commun.* **2018**, *9* (1), 1−9.
(17) Paul, M.; Jons, S. D. Chemistry and Fabrication of Polymeric Nanofiltration Membranes: A Review. *Polymer* **2016**, *103*, 417−456.
(18) Ng, L. Y.; Mohammad, A. W.; Ng, C. Y. A Review on Nanofiltration Membrane Fabrication and Modification Using Polyelectrolytes: Effective Ways to Develop Membrane Selective Barriers and Rejection Capability. *Adv. Colloid Interface Sci.* **2013**, *197−198*, 85−107.
(19) Lau, W. J.; Ismail, A. F.; Misdan, N.; Kassim, M. A. A Recent Progress in Thin Film Composite Membrane: A Review. *Desalination* **2012**, *287*, 190−199.
(20) Wittbecker, E. L.; Morgan, P. W. Interfacial Polycondensation. *J. Polym. Sci.* **1959**, *40* (137), 289−297.
(21) Morgan, P. W.; Kwolek, S. L. Interfacial Polycondensation. II. Fundamentals of Polymer Formation. *J. Polym. Sci.* **1959**, *40* (137), 299.
(22) Freger, V. Nanoscale Heterogeneity of Polyamide Membranes Formed by Interfacial Polymerization. *Langmuir* **2003**, *19* (11), 4791−4797.
(23) Freger, V. Kinetics of Film Formation by Interfacial Polycondensation. *Langmuir* **2005**, *21* (5), 1884−1894.
(24) Zhang, H.; He, Q.; Luo, J.; Wan, Y.; Darling, S. B. Sharpening Nanofiltration: Strategies for Enhanced Membrane Selectivity. *ACS Appl. Mater. Interfaces* **2020**, *12* (36), 39948−39966.
(25) Marchetti, P.; Jimenez Solomon, M. F.; Szekely, G.; Livingston, A. G. Molecular Separation with Organic Solvent Nanofiltration: A Critical Review. *Chem. Rev.* **2014**, *114* (21), 10735−10806.
(26) Saha, N. K.; Joshi, S. V. Performance Evaluation of Thin Film Composite Polyamide Nanofiltration Membrane with Variation in Monomer Type. *J. Membr. Sci.* **2009**, *342* (1−2), 60−69.
(27) Rajaeian, B.; Rahimpour, A.; Tade, M. O.; Liu, S. Fabrication and Characterization of Polyamide Thin Film Nanocomposite (TFN) Nanofiltration Membrane Impregnated with TiO2 Nanoparticles. *Desalination* **2013**, *313*, 176−188.
(28) Lee, S. Y.; Kim, H. J.; Patel, R.; Im, S. J.; Kim, J. H.; Min, B. R. Silver Nanoparticles Immobilized on Thin Film Composite Polyamide Membrane: Characterization, Nanofiltration, Antifouling Properties. *Polym. Adv. Technol.* **2007**, *18* (7), 562−568.
(29) Yang, Z.; Guo, H.; Yao, Z. K.; Mei, Y.; Tang, C. Y. Hydrophilic Silver Nanoparticles Induce Selective Nanochannels in Thin Film Nanocomposite Polyamide Membranes. *Environ. Sci. Technol.* **2019**, *53* (9), 5301−5308.
(30) Ma, X. H.; Yao, Z. K.; Yang, Z.; Guo, H.; Xu, Z. L.; Tang, C. Y.; Elimelech, M. Nanofoaming of Polyamide Desalination Membranes to Tune Permeability and Selectivity. *Environ. Sci. Technol. Lett.* **2018**, *5* (2), 123−130.
(31) Liang, Y.; Zhu, Y.; Liu, C.; Lee, K. R.; Hung, W. S.; Wang, Z.; Li, Y.; Elimelech, M.; Jin, J.; Lin, S. Polyamide Nanofiltration Membrane with Highly Uniform Sub-Nanometre Pores for Sub-1 Å Precision Separation. *Nat. Commun.* **2020**, *11* (1), 1−9.
(32) Bojarska, M.; Gierycz, P.; Religa, P.; Kowalik-Klimczak, A. The Effect of Anionic Surfactant on the Surface Structure of Nanofiltration Membranes. *Challenges Mod. Technol.* **2014**, *5* (2), 33−38.
(33) Mansourpanah, Y.; Madaeni, S. S.; Rahimpour, A. Fabrication and Development of Interfacial Polymerized Thin-Film Composite Nanofiltration Membrane Using Different Surfactants in Organic Phase; Study of Morphology and Performance. *J. Membr. Sci.* **2009**, *343* (1−2), 219−228.
(34) Mansourpanah, Y.; Alizadeh, K.; Madaeni, S. S.; Rahimpour, A.; Soltani Afarani, H. Using Different Surfactants for Changing the Properties of Poly(Piperazineamide) TFC Nanofiltration Membranes. *Desalination* **2011**, *271* (1−3), 169−177.
(35) Duong, P. H. H.; Anjum, D. H.; Peinemann, K. V.; Nunes, S. P. Thin Porphyrin Composite Membranes with Enhanced Organic Solvent Transport. *J. Membr. Sci.* **2018**, *563*, 684−693.
(36) Cui, Y.; Liu, X. Y.; Chung, T. S. Ultrathin Polyamide Membranes Fabricated from Free-Standing Interfacial Polymerization: Synthesis, Modifications, and Post-Treatment. *Ind. Eng. Chem. Res.* **2017**, *56* (2), 513−523.

(37) Azarteimour, F.; Amirinejad, M.; Parvini, M.; Yarvali, M. Organic Phase Addition of Anionic/Non-Ionic Surfactants to Poly(Paraphenyleneterephthalamide) Thin Film Composite Nanofiltration Membranes. *Chem. Eng. Process.* **2016**, *106*, 13−25.
(38) Jiang, C.; Tian, L.; Zhai, Z.; Shen, Y.; Dong, W.; He, M.; Hou, Y.; Niu, Q. J. Thin-Film Composite Membranes with Aqueous Template-Induced Surface Nanostructures for Enhanced Nanofiltration. *J. Membr. Sci.* **2019**, *589* (July), 117244.
(39) Schott, H. Hydrophilic−Lipophilic Balance, Solubility Parameter, and Oil−Water Partition Coefficient as Universal Parameters of Nonionic Surfactants. *J. Pharm. Sci.* **1995**, *84* (10), 1215−1222.
(40) Dinarvand, R.; Moghadam, S. H.; Sheikhi, A.; Atyabi, F. Effect of Surfactant HLB and Different Formulation Variables on the Properties of Poly-D,L-Lactide Microspheres of Naltrexone Prepared by Double Emulsion Technique. *J. Microencapsulation* **2005**, *22* (2), 139−151.
(41) Griffin, W. C. Classification of surface-active agents by" HLB". *J. Soc. Cosmet. Chem.* **1949**, *1*, 311−326.
(42) Chen, G. E.; Liu, Y. J.; Xu, Z. L.; Tang, Y. J.; Huang, H. H.; Sun, L. Fabrication and Characterization of a Novel Nanofiltration Membrane by the Interfacial Polymerization of 1,4-Diaminocyclohexane (DCH) and Trimesoyl Chloride (TMC). *RSC Adv.* **2015**, *5* (51), 40742−40752.
(43) Branzoi, F.; Branzoi, V. Investigation of Some Nonionic Surfactants as Corrosion Inhibitors for Carbon Steel in Sulfuric Acid Medium. *Int. J. Electrochem. Sci.* **2017**, *12* (8), 7638−7658.
(44) Ren, W.; Tian, G.; Jian, S.; Gu, Z.; Zhou, L.; Yan, L.; Jin, S.; Yin, W.; Zhao, Y. TWEEN Coated NaYF 4:Yb,Er/NaYF 4 Core/Shell Upconversion Nanoparticles for Bioimaging and Drug Delivery. *RSC Adv.* **2012**, *2* (18), 7037−7041.
(45) Wenzel, R. N. Surface Roughness and Contact Angle. *J. Phys. Colloid Chem.* **1949**, *53* (9), 1466−1467.
(46) Onaizi, S. A. Dynamic Surface Tension and Adsorption Mechanism of Surfactin Biosurfactant at the Air−Water Interface. *Eur. Biophys. J.* **2018**, *47* (6), 631−640.

https://dx.doi.org/10.1021/acsestengg.0c00213
ACS EST Engg. 2021, 1, 533−542